# Lab on a Chip

Accepted Manuscript






ROYAL SOCIETY OF CHEMISTRY

www.rsc.org/loc

Lab-on-a-Chip RSCPublishing

ARTICLE

# Microfluidic vapor-diffusion barrier for pressure reduction in fully closed PCR modules

Cite this: DOI: 10.1039/x0xx00000x

G. Czilwik[a], I. Schwarz [a], M. Keller [a], S. Wadle [b], S. Zehnle [a], F. von Stetten [a,b], D. Mark [a], R. Zengerle[a,b,c] and N. Paust [a,b]

Received 00th January 2012,
Accepted 00th January 2012

DOI: 10.1039/x0xx00000x

www.rsc.org/

Microfluidic systems for polymerase chain reaction (PCR) should be fully closed to avoid vapor loss and to exclude the risk of contaminating the laboratory environment. In closed systems however, the high temperatures of up to 95°C associated with PCR cause high overpressures up to 100 kPa, dominated by the increase of vapor partial pressure upon evaporation. Such high overpressures pose challenges to the mechanical stability of microfluidic chips as well as to the liquid handling in integrated sample-to-answer systems. In this work, we drastically reduce the pressure increase in fully closed PCR systems by integrating a microchannel that serves as a vapor-diffusion barrier (VDB), separating the liquid-filled PCR chamber from an auxiliary air chamber. In such configurations, propagation of vapor from the PCR chamber into the auxiliary air chamber and as a consequence the increase of pressure is limited by the slow diffusion process of vapor through the VDB. At temperature increase from 23°C to 95°C, we demonstrate the reduction of overpressure from more than 80 kPa without the VDB to only 35 kPa with the VDB. We further demonstrate proper function of VDB and its easy integration with downstream processes for PCR based nucleic acid amplification within centrifugal microfluidics. Without integration of the VDB, malfunction due to pressure-induced delamination of the microfluidic chip occurred.

## Introduction

Microfluidic platforms allow easy, fast, and cost-efficient automation of various bioassay processes[1] for realization of 'micro total analysis systems', or 'Lab-on-a-Chip'(LoaC)[2,3]. Several reviews are available that present applications for point-of-care diagnostics[4–6], or specifically addressing immunosensors[7] and nucleic acid analysis[8]. Polymerase chain reaction (PCR) has been the gold standard for nucleic acid amplification-based analysis for decades, and is applied in many LoaC-systems[8–12]. PCR requires a thermal denaturation step of DNA with liquid temperatures of about 95°C, causing degassing of dissolved gas and evaporation of the involved liquids. Consequently, bubbles form and pressure increases significantly, due to the increase of partial pressures of vapor and heated air. To compensate for overpressure and to reduce evaporation, liquid phase change microvalves[13], elastomer valves[14], open air vents[15–17] or oil sealings[18,19] have been applied. Whereas open air vents may lead to vapor loss and bear the risk of contaminating the laboratory environment, liquid phase change or elastomer valves increase the complexity of integration and fabrication. Adding oil leads to a reduced choice of reaction vessels or microfluidic chip fabrication substrates due to solubility of many polymers in mineral oils. Furthermore, oil usage is incompatible with UV-treatment of the reaction vessels, which is done to destroy DNA contaminations that may cause false positive test results[20,21]. Third, compatibility of the oil with the PCR reagents must be carefully evaluated. At last, presence of mineral oil can impair downstream processes after PCR, such as further liquid processing, cloning or product analysis[22].

In this work, a novel principle to reduce the pressure increase in closed LoaC PCR systems is introduced and investigated, theoretically as well as experimentally. The novel principle relies on separation of a PCR chamber (liquid compartment) from an auxiliary air chamber (air compartment) by a microchannel that serves as a vapor-diffusion-barrier (VDB). VDBs have been already employed to reduce vapor loss from low volume PCR reactions[23,24] in open systems, however, they have not been exploited to intentionally reduce the transient pressure increase within a hermetically sealed microfluidic network.

In our study, we provide a model equation that allows for predicting the pressure increase caused by the partial pressures of air and vapor in dependency of time and the VDBs geometry. We validate the model equation using an experimental setup with six different VDB geometries. For experimental characterization, we applied the VDB structures on the centrifugal microfluidic LabDisk platform[25–30].

The platform features inertial liquid propulsion by rotation,

eliminating the need of any interfaces to external pumps. This enables closed and contamination free fluidic systems in an easy manner. In addition, bubbles formed during heating of liquid are inherently separated by centrifugal buoyancy rendering the platform an ideal candidate for integrated PCR analysis[15,16]. We proofed the proper function of VDB's by applying them in a structure for PCR based pre-amplification, which is usually used to achieve lower detection limits in geometrically multiplexed PCR[31,32] or to enable the direct use of crude samples rendering nucleic acid purification redundant[33].

To demonstrate easy integration with further downstream processes, subsequently to the PCR amplification the reaction product is pumped radially inwards employing a centrifugo-dynamic pumping mechanism[34]. The complete integration of microfluidic pre-amplification significantly lowers the risk of cross-contamination in a laboratory environment that may be caused by manually handling high copy numbers of DNA after amplification.

Finally, we compare a first embodiment of a chamber without separation of liquid and air compartments to a second embodiment where the main fraction of air is located within an auxiliary air chamber ("Chamber B") that is separated from the liquid compartment ("Chamber A") by a VDB (see Figure 1 a,b). Thereby, the pressure stability is investigated using pressure sensitive adhesive (PSA) foils which are frequently used as sealings for LoaC [35–37].

## Theory

PCR setups usually contain a two phase configuration - an air volume above a liquid volume - as depicted in Fig. 1a. When heating up such a system close to the boiling temperature, approximately 80% of the pressure increase is caused by the increase of partial pressure of vapor and approximately 20% relates to the increase of partial pressure of air. Therefore, a good strategy for pressure reduction is to reduce the overall vapor content within the system. This can be achieved by separating a liquid compartment from an air compartment by a vapor-diffusion barrier as depicted in Fig. 1b.

In the following, we consider a chamber A (PCR chamber) filled with liquid, a chamber B (pneumatic chamber) filled with air and a VDB microchannel connecting chamber A with chamber B. The liquid-air interface is located within chamber A, as depicted in Fig. 1b. When the structure is heated, the pressure in chamber B increases according to the ideal gas law for air resulting in a pressure increase of about 20%. The same happens in chamber A, but here also vapor is created that leads to additional vapor pressure above the interface. Therefore, a pressure gradient from chamber A to B is formed that results in convective transport of a certain volume of air and vapor through the VDB towards chamber B. As a consequence, air above the liquid interface depletes and the partial pressure of air in chamber A reduces. The convective transport stops as soon as the sum of partial pressure of air and vapor in chamber A is equal to the pressure in chamber B. The key to VDB mediated pressure reduction is that the air volume in chamber A is very small compared to the air volume in chamber B. Therefore, equilibrium of pressure is reached with very little convective transport within a very short time and the overall convection can be neglected for the theoretical description of pressure increase.

The functionality of the VDB can thus be explained as follows. Assuming a temperature $T$ above room temperature, liquid evaporates until the air next to the liquid interface is saturated with vapor, with the partial pressure of the vapor reaching $p(T)$. A concentration gradient of the vapor species between the liquid-air interface and chamber B forms and Brownian molecular motion causes transport of vapor away from the liquid-air interface into chamber B. Assuming a fully developed concentration profile, the transport of the vapor species can reasonably be approximated by a one dimensional quasi-static model using the first Fick's law:

$$J = -\mathrm{AD}\frac{\partial c}{\partial \mathrm{x}} \tag{1}$$

where $J$ is the molar flow of vapor along the microchannel, $A$ the channel cross-section, $D$ the diffusion coefficient for the vapor in air, $c$ the concentration of vapor in the air phase and $x$ the coordinate along the microchannel. The concentration gradient is approximated by assuming vapor saturated air at the liquid interface in chamber A and a homogenous vapor concentration $c$ in chamber B, thus, the gradient yields:

$$\frac{\partial c}{\partial x} = \frac{c^B - c^S(T)}{L} \tag{2}$$

with $c^S(T)$ as the saturated vapor concentration above the liquid-air interface in chamber A, $c^B$ as the average concentration of vapor in the air of chamber B and $L$ as the length of the microchannel. According to the continuity equation, the molar inflow J into chamber B leads to a change in vapor concentration in chamber B. Both are connected via:

$$J = \mathrm{V}_B \frac{\partial c^B}{\partial t} \tag{3}$$

Thus, combining Eq. 1 to Eq. 3 and reformulating leads to:

$$\frac{\partial c^B}{\partial t} = \frac{1}{V_B} A\, D\, \frac{c^S(T) - c^B(t)}{L}. \tag{4}$$

The partial pressure of vapor in chamber B is linked to the vapor concentration $c^B$ via the ideal gas law: $p^B_{vap}(T) = \mathrm{c^B}\ \mathrm{RT}$. It can be calculated via integrating equation (4) and results in:

$$p^B_{vap}(T) = T\, R(c^S(T) + \left(c^B(t_0) - c^S(T)\right)e^{\frac{-A\,D\,t}{L\,V_B}}) \tag{5}$$

The absolute pressure in chamber B is the sum of the partial pressures. The partial pressure of air can be calculated via the ideal gas law at constant volume and depends on the temperature, only. Finally the pressure rise in chamber B results in:

$$p(t,T) = p^{id.gas}_{air}(T) + T\, R(c^S(T) + \left(\mathrm{c}(t_0) - c^S(T)\right)e^{\frac{-A\,D\,t}{L\,V_B}}) \tag{6}$$

At a given temperature $T$ as a boundary condition for a bio-chemical reaction, the pressure increase can be limited by adjusting $\frac{A}{L\,V_B}$. In other words, increasing the volume $V_B$ of chamber B, decreasing the channel cross-section $A$ of the VDB channel or increasing the length $L$ has the same effect of slowing down the increase of pressure due to evaporation.

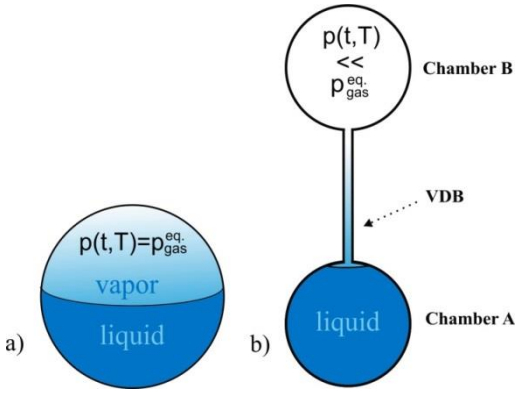


**Figure 1** - Schematic view of fluidic structures with a liquid-air mixture at a time *t* after an initial heating step. a) The vapor-liquid equilibrium is rapidly reached by diffusion and convection in a closed cavity. b) A capillary prevents rapid propagation of vapor. The time frame until the equilibrium of vapor-liquid is reached is greatly enhanced.

## Material and methods

### LabDisk design and microfluidic processing

The basic microfluidic design for our test structure is derived from our previous work for centrifugo-dynamic pumping[34]. The pumping is based on enclosing and compressing an air bubble in a dead-end chamber during centrifugation. Thereby, pneumatic energy is stored. Upon lowering centrifugation, the air decompresses and the pneumatically stored energy is released, which is employed to pump liquid. In contrast to our previous work, we separate the chambers for the liquid (here termed PCR chamber) and the compressed air (pneumatic chamber) with the VDB channel as schematically depicted in Figure 2. The PCR chamber is designed to match the liquid volume of the PCR reaction mix. As in the previous work, the inlet chamber is connected to the PCR chamber with a narrow inlet channel with high fluidic resistance and with a wider outlet channel with low fluidic resistance which enables the centrifugo-dynamic pumping.

For a first experimental set-up, six structures with different cross-sections of the VDB channel were integrated on LabDisk 1a (depicted in Figure S1 in the electronic supplement). The sum of the pneumatic chamber volume and VDB-channel volume (the effective air-compression volume) are equal in all structures and add up to 440.0 µL. The volume of the PCR chamber is 42.0 µL. LabDisk 1a was used for model validation and for determination of overpressures at different temperatures and during thermocycling. To study generation of overpressures for smaller liquid volumes, three different structures with PCR chamber volumes of 21.0 µL, 10.5 µL, and 5.3 µL were integrated on LabDisk 1b (depicted in Figure S2 in the electronic supplement). For this purpose, the VDB and the volumes of the pneumatic chamber have been scaled down according to structure 1 of LabDisk 1a, keeping the same ratio between the PCR chamber and the pneumatic chamber and between the PCR chamber and the cross-section of the VDB. The most important geometric data of LabDisk 1a and 1b is listed in Table 1. Another test carrier, LabDisk 2, was designed to demonstrate the PCR application and the compatibility of the VDB structure with downstream processing such as centrifugo-dynamic pumping. LabDisk 2 (depicted in Figure S3 in the electronic supplement)

Table 1 – LabDisk 1a: Effective cross-section of VDB channels for structure 1-6. The factor expresses the relation between the cross section of each VDB to the smallest cross section (VDB of structure 1). LabDisk 1b: Volume of the PCR chamber and the pneumatic chamber and cross-section of the VDB for structures 7-9. The length of all VDB channels is 9.3 mm.

| **LabDisk 1a** | | |
|---|---|---|
| **Structure** | **Factor** | **Cross-section *A* of VDB** |
| 1 | 1 | 106 µm x 88 µm |
| 2 | 2 | 160µm x 120 µm |
| 3 | 4 | 200 µm x 187 µm |
| 4 | 8 | 300 µm x 250 µm |
| 5 | 16 | 400 µm x 374 µm |
| 6 | 32 | 600 µm x 500 µm |

| **LabDisk 1b** | | | |
|---|---|---|---|
| **Structure** | **Volume PCR chamber** | **Volume pneumatic chamber** | **Cross-section A of VDB** |
| 7 | 21.0 µL | 220.0 µL | 84 µm x 55 µm |
| 8 | 10.5 µL | 110.0 µL | 54 µm x 43 µm |
| 9 | 5.3 µL | 55.0 µL | 42 µm x 28 µm |

features two structures. The first structure uses a 100 µm x 100 µm VDB channel with a length of 15.1 mm that connects the pneumatic chamber hosting 223.0 µL to the PCR chamber of 42.0 µL. The second structure is designed for reference and does not apply a VDB channel; hence the pneumatic and PCR chambers are combined to a total volume of 265.0 µL. Both structures have an outlet chamber that is connected to an additional chamber of 1.5 mL volume (not included in Figure 2). This additional air volume ensures a relatively lower air compression in the outlet chamber during the post-PCR centrifugo dynamic pumping process. The lower air compression in the outlet structure allows for relatively high pump efficiencies. In

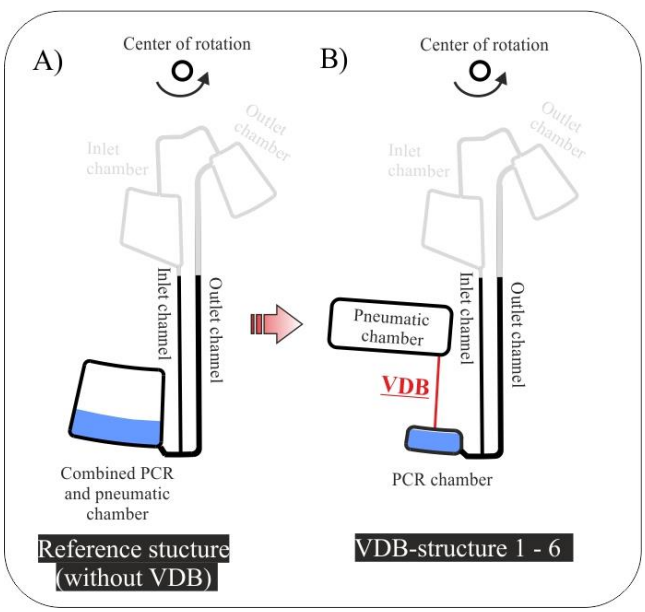


**Figure 2.** Schematic of the vapor diffusion barrier mediated pressure reduction during PCR thermocycling. a) Reference structure without VDB. b) The pneumatic chamber is separated from the PCR chamber. Both chambers are connected by the VDB channel. Structures 1 - 6 differ only in the dimension of the cross-section of the VDB, according to Table 1.

this context, the pump efficiency is defined as the ratio of the liquid volume pumped into the outlet chamber ($V_{pumped}$) to the total liquid volume ($V_{total}$):

$$\text{pump efficiency } \eta = \frac{V_{pumped}}{V_{total}}. \quad (7)$$

**LabDisk fabrication**

All designs were manufactured in-house by HSG-IMIT Lab-on-a-Chip Design and Foundry Service (www.loac-hsg-imit.de/en/design-foundry-service) according to our previously reported micro-thermoforming process[38]. In short, the channels were milled into a 4 mm PMMA substrate (Plexiglas, Evoniks, Germany) using CNC micromilling (Micro- und Feinwerktechnik GmbH & Co. KG, Germany, Type MMP 2522). The milled PMMA structures were each casted with PDMS (Elastosil RT607, Wacker, Germany) to obtain a negative mold insert for blow molding. The mold inserts were used to replicate LabDisk 1a and LabDisk 1b using 200 µm thick cyclic olefin copolymer foils (COC 6013/8007, Topas) by blow molding. LabDisk 1a and LabDisk 1b were sealed with a 160 µm thick cyclic olefin polymer foil (COC 6013/8007, Topas) using pressure-assisted thermal sealing. LabDisk 2 was replicated using 188 µm thick cyclic olefin polymer foils (COP ZF14, Zeonex). Subsequently, LabDisk 2 was sealed using a pressure sensitive adhesive (PSA) polyolefin foil (#900320, HJ Bioanalytik, Germany). As stated above, two different sealing technologies of the LabDisks were used. Providing thermally bonded sealings that withstand even high overpressures above 100 kPa, LabDisk 1a and LabDisk 1b were used to validate the functionality of the VDB and to provide evidence for the theoretical model. LabDisk 2 was used as an application example for the VDB enabling PCR in cartridges that are subject to mal-function e.g. by pressure-induced delamination of an adhesive sealing foil.

**Processing device and measurement setup**

Processing of the LabDisks was performed in a LabDisk Player (QIAGEN Lake Constance, Stockach, Germany), a prototype device that allows for full control over rotational frequency, acceleration and temperature. The LabDisk is herein mounted on a rotational axis within a processing chamber. The temperature of the processing chamber is controlled with a heating and cooling mechanism that is based on convection of hot air and ambient air, respectively. Heating of circulating air is realized with heating wires whereas ambient air is used for cooling. The temperature is controlled with a rotary valve that regulates influx of ambient air and release of internally heated air. To visualize the liquid-flow in the rotating LabDisk, the LabDisk player was equipped with a customized stroboscopic image acquisition system[39] (Biofluidix GmbH, Germany).

**Preparation of DNA for PCR amplification**

DNA was extracted from an *Escherichia coli* suspension that was cultured overnight at 37°C in lysogenic broth medium (catalog number L3022, Sigma-Aldrich, Germany) in an incubator. The DNA was extracted using a commercial kit (ajInnuscreen, Berlin, Germany) according to the manufacturers protocol.

**Experimental**

For investigation of the pressures in LabDisks 1a and 1b respectively, all experiments were conducted using distilled water ($dH_2O$) (UltraPure™ DNase/RNase-Free Distilled Water, Life Technologies, USA). For the PCR amplification on LabDisk 2, a commercially available PCR mix (illustra Hot Start Mix RTG, GE Healthcare, USA) was used. To determine the pressure in the pneumatic chambers of LabDisks 1a and 1b respectively, images were acquired with the stroboscopic setup, which were subsequently analysed using ImageJ software (Version V1.48b, NIH, USA).

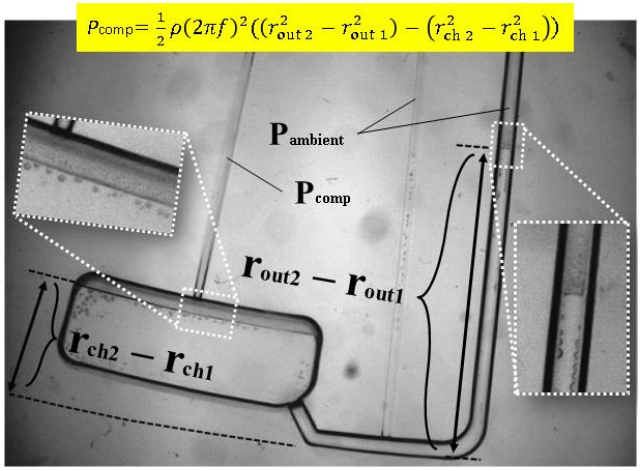


**Figure 3** - Pressure calculation in the pneumatic chamber by determination of the hydrostatic pressures. For this purpose, the difference of the liquid level in the PCR chamber to the liquid level in the vented outlet channel is measured. The liquid-air interfaces in the PCR chamber and in the outlet channel are highlighted in the boxes (white dashed lines).

The height of the liquid columns in the outlet channel and the PCR chamber were determined, as depicted in Figure 3, which directly correlates with the pressure in the pneumatic chamber as follows:

$$p_{\text{comp}} = \frac{1}{2}\rho(2\pi f)^2((r_{out\,2}^2 - r_{out\,1}^2) - (r_{ch\,2}^2 - r_{ch\,1}^2)), \quad (8)$$

where $\rho$ is the density of the liquid, $f$ the spinning frequency, $r_{\text{out}\,2}$ and $r_{\text{out}\,1}$ are the outermost and innermost radii of the liquid column in the outlet channel and $r_{\text{ch}\,2}$ and $r_{\text{ch}\,1}$ are the outermost and innermost radii of the liquid column in the PCR chamber, respectively.

To observe pressure increase over time at a constant elevated temperature, LabDisk 1a was placed in the processing chamber of the player and the complete setup was preheated to 80°C for 15 minutes prior to testing. Afterwards, 40 µL of $dH_2O$ was loaded at each inlet chamber. The lid of the processing chamber of the LabDisk player was closed and the LabDisk 1a was first rotated for 2 minutes at 2 Hz and 80°C air temperature. With low centrifugal pressure, the liquid does not yet enter the PCR chamber and the LabDisk is given enough time to reach a constant temperature level after liquid loading. Subsequently, LabDisk 1a was accelerated to 40 Hz (acceleration rate 10 Hz $s^{-1}$) to fill the PCR chamber thereby compressing air in the pneumatic chamber. At a constant temperature of 80°C, the pressure in the pneumatic chambers was then constantly monitored for 30 minutes.

The thermocycling protocol that was used for pressure characterization tests with LabDisk 1a and 1b respectively, and pumping tests with LabDisk 2 included a denaturation step at 95°C (30 s), an annealing step at 60°C (45 s) and an elongation step at 72°C (30 s). For PCR amplification with LabDisk 2, an additional polymerase activation step at 95°C (120 s) with subsequent identical thermocycles was used.

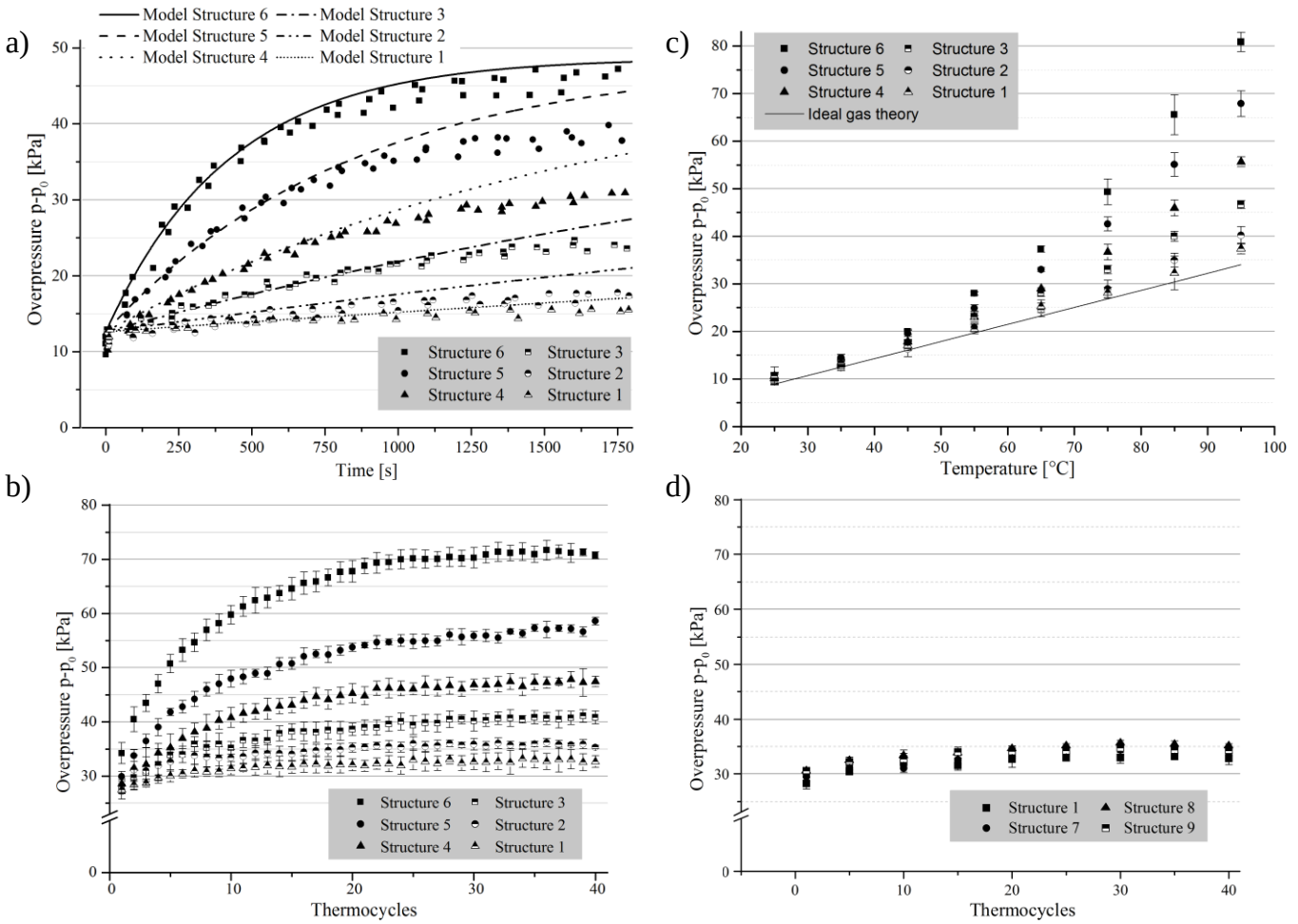


**Figure 4 - Overpressure in pneumatic chamber** a) Overpressure over time at a constant temperature of 80°C. The model parameters for computation of the overpressure according to equation (6) are the diffusion coefficient $D$ of vapor in air of 3.24 x $10^5$ $m^2$ $s^{-1}$, the saturated vapor concentration $\boldsymbol{c^s(T)}$of 13.20 mol $m^{-3}$, and the initial vapor concentration $\boldsymbol{c(t_0)}$ of 0.835 mol $m^{-3}$ in the pneumatic chamber. b) Overpressure between 25°C to 95°C. The standard deviations of the pressure of three experiments are depicted as error bars. c) Evolution of pressure in pneumatic chamber at the denaturation step for 40 thermocycles. For thermocycling a specifically developed PCR temperature control model was applied to allow for fast cycling. For heating and cooling over- and undershoots are employed to reach an average heating rate of 1 K/s. The overpressures generated within the first three cycles indicate that temperature of 95°C is not fully reached by the processing device. The standard deviations of the pressure of three experiments are depicted as error bars. d) Evolution of pressure in pneumatic chambers at the denaturation step for 40 thermocycles for PCR chamber volumes of 42.0 µL (structure 1), 21.0 µL (structure 7), 10.5 µL (structure 8) and 5.3 µL (structure 9).

## Results and discussion

### Pressure characterization

The pressure increase over time in the pneumatic chamber for the six different VDB configurations of LabDisk 1a as listed in Table 1 is plotted in Figure 4a. The trend of significantly slower pressure increase with smaller cross-sections of the VDB channel is clearly visible. Comparison with theoretical values calculated based on equation (6) shows good agreement within the first approximately 900 seconds. Later, the pressure increase of the measured values is somewhat below the theoretical expected progress. A possible explanation is that vapor and air diffuse through the foil base material causing a slightly slower pressure increase. A model addressing such phenomena would have to cope with transport phenomena within the complex geometry of the blow molded solid material and is beyond the scope of this work, in particular because for PCR applications, relevant holding times at elevated temperatures above 90°C are 900 seconds maximum for an initial hot start. Using LabDisk 1a, also the pressure in the pneumatic chambers for the temperature range of 25°C – 95°C was determined. The temperature was raised from 25°C to 95°C in steps of 10°C. At each temperature step, measurements of the pressure were determined 5 minutes after reaching the set air temperature value. The 5 minutes holding time was used to ensure that the set temperatures are fully reached as, in contrast to thermocycling, no overshooting of temperature for fast heating was applied. The results are plotted in Figure 4b.

The initial overpressure at 25°C is equal for all structures and corresponds to the pressure by compression of air according to the ideal gas law:

$$p_{\mathrm{comp}}(V) - p_0 = p_0\left(\left(\frac{V_0}{V_0 - \Delta V}\right) - 1\right), \qquad (9)$$

where $p_0$ is ambient pressure, $V_0$ is the effective gas volume of the pneumatic and PCR chambers and $\Delta V$ is the liquid volume. As temperature increases, the pressure increases as well as indicated by

the solid line of Figure 4b, again according to the ideal gas law now considering temperature instead of volume changes:

$$p^2_{comp}(T) - p^1_{comp} = p^1_{comp}(\frac{T}{T_0} - 1), \quad (10)$$

where $T$ indicates the temperature in the processing chamber and $T_0$ is the initial temperature (here room temperature). Whereas structures 1 and 2 almost comply with the ideal gas law, indicating that almost no vapor is present inside the pneumatic chamber and thus the influence of partial pressure of vapor is negligible, structure 3 and 4 already show significant influence by vapor generation. The highest overpressures in the temperature range, as expected, is observed for the largest cross-section of structure 6 with a maximum overpressure of 81 kPa ± 2 kPa at a temperature of 95°C.

After model validation and VDB characterization at constant temperatures, it was investigated how pressure evolves for a thermocycling protocol that is typically used for PCR amplification. For this purpose, 40 thermocycles were conducted with LabDisk 1a at constant rotation at 40 Hz. The pressures at the denaturation step of each thermocycle are depicted in Figure 4c. Again, the correlation between pressure increase and the cross-section of the VDB-channel can be clearly observed. The maximum pressure occurred in structure 6 (largest cross-section) of the VDB, whereas the minimum pressure was generated for structure 1 (smallest cross-section).

For all structures, pressures have reached steady-state after approximately 25 thermocycles. After 40 thermocycles, liquid volumes in the PCR chambers were measured showing a volume reduction of approximately 4.5 µL for structure 6 (largest cross-section), whereas for structure 1 (smallest cross-section), a liquid volume reduction of approximately 0.5 µL was observed. Consequently, the volume loss increases for larger dimensions of the VDB. This can be explained by vapor transport through the foil material which itself depends on the overpressure. The higher volume loss for larger VDB cross-sections supports the assumption that steady-state is caused by an equilibrium of diffusive vapor transport through the VDB into the pneumatic chamber on the one hand, and gas diffusion through the foil material out of the pneumatic chamber on the other hand. In structure 6, the large cross-section of the VDB causes a comparatively fast vapor transport into the pneumatic chamber and thus a relatively higher pressure increase, which in turn enhances diffusive vapor transport through the foil. Steady-state is thus reached on a comparatively high pressure level (71 kPa). In contrast, the small VDB cross-section of structure 1 significantly reduces vapor transport into the pneumatic chamber, which results in a comparatively lower pressure increase. Consequently, the pressure dependent vapor loss through the foil is lower and the steady-state is reached on a relatively lower pressure level (33 kPa).

Finally we investigated how pressure evolves for the scaled-down structures of LabDisk 1b with varying PCR chamber volumes of 21.0 µL, 10.5 µL and 5.3 µL. Figure 4d shows the results of pressure generation in the pneumatic chambers at the denaturation step during the 40 thermocycles. As expected, the pressures of all structures throughout the 40 thermocycles only vary within a range of approximately 3-4 kPa, demonstrating the scalability of our VDB principle to smaller volumes.

**PCR amplification on LabDisk 2 with subsequent transport of the amplification product for downstream processing**

The implementation of PCR amplification with a VDB in a centrifugal microfluidic network was demonstrated with LabDisk 2. First, we conducted experiments with PCR buffer without primers to check whether the PSA foil could withstand the pressure generated during PCR thermocycling. Malfunction was observed for the structure without application of a VDB in 3 out of 3 experiments as the sealing foil delaminated already during the first denaturation steps (Figure 5). Using the structure with the VDB channel (cross-section of 100 µm x 100 µm and a length of 15.1 mm) the structure was fully functional and did not show any signs of delamination even after 40 thermocycles. Thereafter, the same VDB-structure of LabDisk 2 was used to conduct PCR amplification. Primers (sequences described in section 4 of electronic supplement) in a final concentration of 0.2 µM were used to amplify a sequence in the *PAL* gene region of *Escherichia coli* using 30 thermocycles. 1 ng of genomic DNA of *Escherichia coli* was used as sample DNA. After finishing thermocycling, the amplification product was transferred radially inwards from a radial position of 60.0 mm over a radial distance of 43.1 mm to a collection chamber by centrifugo-dynamic pumping. The amplification product was recovered manually using a pipette. The amplification products of three consecutive runs with the VDB structure were successfully detected on a 1% agarose gel pre-stained with ethidium-bromide (data not shown). To quantify the pumping efficiency, thermocycling experiments were carried out with PSA-sealed venting holes, thereby incorporating a fully closed setup. The principle of inward pumping is described in Figure S4 in the electronic supplement. We conducted 20 thermocycles at a constant rotational frequency of 40 Hz. After thermocycling, inward pumping was performed at 2 Hz at a constant temperature of 75°C. Throughout three experiments the pumping efficiency was 84.6 % ± 4.8 %.

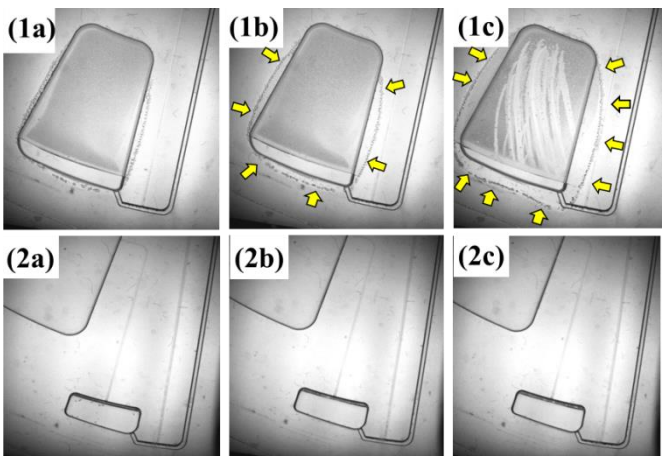


**Figure 5 – (1a-1c):** Delamination without application of a VDB channel. The delamination process is illustrated with yellow arrows. The status is shown at 95°C at the first (1a), second (1b), and third (1c) denaturation step. **(2a-2c):** VDB mediated pressure reduction prevents delamination. Structure with VDB channel: (2a) First denaturation step, (2b) 20$^{th}$ denaturation step. And (2c) 40$^{th}$ denaturation step. No delamination was observed.

## Conclusions

In this paper we introduced a new method of passively reducing the pressure increase due to evaporation of liquid at elevated temperatures in fully closed two-phase microfluidic systems. The key element is the application of a vapor diffusion barrier (VDB) channel separating liquid compartments from air compartments to decrease vapor pressure generation in closed liquid-air configurations as used e.g. for PCR-based assays. The VDB mediated pressure reduction significantly reduces demands on manufacturing as well as on system integration and reduces possible evaporation through the bulk material. This evaporative loss may be of particular interest if small volumes (<5 µL) are applied for PCR amplifications.

As an application example for vapor diffusion barrier mediated pressure reduction, the PCR based nucleic acid amplification as well as the subsequent transport of the amplification product was demonstrated on a centrifugal microfluidic LabDisk.

In principle the VDB mediated pressure reduction can be employed on different (microfluidic) platforms e.g. on pressure driven systems. In this context, special care must be taken to avoid any liquid from entering the VDB, which would lead to blockage of the VDB by liquid plugs. Such blockage could be avoided by specific geometric constrictions such the integration of phase guides[40] or by applying local hydrophobic coatings.

VDB mediated pressure reduction can be applied to all applications with two-phase configurations where reduced pressure at elevated temperatures is desired. Here, besides all applications requiring thermal DNA denaturation, the thermal lysis of microorganisms should be mentioned. Within centrifugal microfluidics, the VDB is especially relevant if operations at elevated temperatures have to be combined with downstream steps such as the PCR pre-amplification with a subsequent geometric multiplexed PCR[31,32].

Using the theoretical model introduced in this work, the overpressure in unvented chambers that are connected to a liquid compartment via VDB can be predicted. A next step would be to apply the model in network-based computational modelling for efficient layout of complete microfluidic networks. In the long term, the presented VDB concept facilitates easily fabricated, fully integrated and fully closed microfluidic chips for the implementation of more and more complex assay protocols at elevated temperatures.

## Acknowledgements

The research leading to these results has received funding from the European Union's Seventh Framework Programme (FP7/2007-2013) under grant agreement n° 258759.

## Notes and references

[a] HSG-IMIT – Institut für Mikro- und Informationstechnik, Georges-Koehler-Allee 103, 79110 Freiburg, Germany. Email: gregor.czilwik@hsg-imit.de .

[b] Laboratory for MEMS Applications, IMTEK - Department of Microsystems Engineering, University of Freiburg, Georges-Koehler-Allee 103, 79110 Freiburg, Germany

[c] BIOSS – Centre for Biological Signalling Studies, University of Freiburg, 79110 Freiburg, Germany

Electronic Supplementary Information (ESI) available: Design of LabDisk 1a, design of LabDisk 1b and design of LabDisk 2, Inward pumping principle with LabDisk 2, PCR primers.

1 D. Mark, S. Haeberle, G. Roth, F. von Stetten, and R. Zengerle, *Chem. Soc. Rev.*, 2010, 39, 1153–82.
2 A. Manz, N. Graber, and H. M. Widmer, Sensor*s Actuators B Chem.*, 1990, 1, 244–248.
3 D. Janasek, J. Franzke, and A. Manz, *Nature*, 2006, 442, 374–80.
4 P. Yager, T. Edwards, E. Fu, K. Helton, K. Nelson, M. R. Tam, and B. H. Weigl, *Nature*, 2006, 442, 412–8.
5 C. a Holland and F. L. Kiechle, *Curr. Opin. Microbiol.*, 2005, 8, 504–9.
6 C. D. Chin, V. Linder, and S. K. Sia, *Lab Chip*, 2012, 12, 2118–34.
7 M.-I. Mohammed and M. P. Y. Desmulliez, *Lab Chip*, 2011, 11, 569–95.
8 C.-M. Chang, W.-H. Chang, C.-H. Wang, J.-H. Wang, J. D. Mai, and G.-B. Lee, *Lab Chip*, 2013, 13, 1225–42.
9 Y. Zhang and P. Ozdemir, *Anal. Chim. Acta*, 2009, 638, 115–25.
10 A. M. Foudeh, T. Fatanat Didar, T. Veres, and M. Tabrizian, *Lab Chip*, 2012, 12, 3249–66.
11 J. M. Bienvenue, L. A Legendre, J. P. Ferrance, and J. P. Landers, *Forensic Sci. Int. Genet.*, 2010, 4, 178–86.
12 J. a Lounsbury, A. Karlsson, D. C. Miranian, S. M. Cronk, D. a Nelson, J. Li, D. M. Haverstick, P. Kinnon, D. J. Saul, and J. P. Landers, *Lab Chip*, 2013, 13, 1384–93.
13 R. Pal, M. Yang, B. N. Johnson, D. T. Burke, and M. A Burns, *Anal. Chem.*, 2004, 76, 3740–8.
14 N. M. Toriello, C. N. Liu, and R. A. Mathies, *Anal. Chem.*, 2006, 78, 7997–8003.
15 M. Focke, F. Stumpf, G. Roth, R. Zengerle, and F. von Stetten, *Lab Chip*, 2010, 10, 3210–2.
16 S. Lutz, P. Weber, M. Focke, B. Faltin, J. Hoffmann, C. Müller, D. Mark, G. Roth, P. Munday, N. Armes, O. Piepenburg, R. Zengerle, and F. von Stetten, *Lab Chip*, 2010, 10, 887–893.
17 O. Strohmeier, N. Marquart, D. Mark, G. Roth, R. Zengerle, and F. von Stetten, *Anal. Methods*, 2014.
18 J. H. Daniel, S. Iqbal, R. B. Millington, D. F. Moore, C. R. Lowe, D. L. Leslie, M. A. Lee, and M. J. Pearce, *Sensors Actuators A Phys.*, 1998, 71.
19 G. R. M. Duarte, C. W. Price, B. H. Augustine, E. Carrilho, and J. P. Landers, *Anal. Chem.*, 2011, 83, 5182–9.
20 M. Gilgen, C. Höfelein, J. Lüthy, and P. Hübner, *Nucleic Acids Res.*, 1995, 23, 4001–2.
21 G. L. Dohner DE, Dehner MS, Biotechniques, 1995, 18(6):964-.
22 B. Hébert, J. Bergeron, E. F. Potworowski, and P. Tijssen, *Mol. Cell. Probes*, 1993, 7, 249–52.
23 F. Wang, M. Yang, and M. a Burns, *Lab Chip*, 2008, 8, 88–97.
24 C. Zhang and D. Xing, *Microfluid. Nanofluidics*, 2009, 9, 17–30.
25 R. Gorkin, J. Park, J. Siegrist, M. Amasia, B. S. Lee, J.-M. Park, J. Kim, H. Kim, M. Madou, and Y.-K. Cho, *Lab Chip*, 2010, 10, 1758–73.
26 J. Ducrée, S. Haeberle, S. Lutz, S. Pausch, F. Von Stetten, and R. Zengerle, *J. Micromechanics Microengineering*, 2007, 17, S103–S115.

27 Y.-K. Cho, J.-G. Lee, J.-M. Park, B.-S. Lee, Y. Lee, and C. Ko, *Lab Chip*, 2007, 7, 565–73.
28 B. S. Lee, J.-N. Lee, J.-M. Park, J.-G. Lee, S. Kim, Y.-K. Cho, and C. Ko, *Lab Chip*, 2009, 9, 1548–55.
29 A. Kazarine, M. C. R. Kong, E. J. Templeton, and E. D. Salin, *Anal. Chem*., 2012, 84, 6939–6943.
30 D. A. Duford, Y. Xi, and E. D. Salin, *Anal. Chem*., 2013, 85, 7834–7841.
31 E. Aurelius, B. Johansson, B. Sköldenberg, a Staland, and M. Forsgren, *Lancet*, 1991, 337, 189–92.
32 P. A Rachwal, H. L. Rose, V. Cox, R. A Lukaszewski, A. L. Murch, and S. A Weller, *PLoS One*, 2012, 7, e35971.
33 S. H. Lee, V. S. Vigliotti, and S. Pappu, *BMC Womens Health*, 2009, 9, 8.
34 S. Zehnle, F. Schwemmer, G. Roth, F. von Stetten, R. Zengerle, and N. Paust, *Lab Chip*, 2012, 12, 5142–5.
35 N. Godino, R. Gorkin, A. V Linares, R. Burger, and J. Ducrée, *Lab Chip*, 2013, 13, 685–94.
36 O. Strohmeier, A. Emperle, G. Roth, D. Mark, R. Zengerle, and F. von Stetten, *Lab Chip*, 2013, 13, 146–55.
37 J. Siegrist, R. Gorkin, M. Bastien, G. Stewart, R. Peytavi, H. Kido, M. Bergeron, and M. Madou, *Lab Chip*, 2010, 10, 363–71.
38 M. Focke, F. Stumpf, B. Faltin, P. Reith, D. Bamarni, S. Wadle, C. Müller, H. Reinecke, J. Schrenzel, P. Francois, D. Mark, G. Roth, R. Zengerle, and F. von Stetten, *Lab Chip*, 2010, 10, 2519–26.
39 M. Grumann, T. Brenner, C. Beer, R. Zengerle, and J. Ducrée, *Rev. Sci. Instrum*., 2005, 76, 025101.
40 P. Vulto, S. Podszun, P. Meyer, C. Hermann, A. Manz, and G. A.Urban, *Lab Chip, 2011, 11, 1596–1602.*
41 F. Goldschmidtboeing, M. Rabold, and P. Woias, *J. Micromechanics Microengineering, 2006, 16, 1321–1330.*



 